Hindawi Publishing Corporation
Journal of Nanomaterials
Volume 2015, Article ID 347486, 9 pages
http://dx.doi.org/10.1155/2015/347486

Research Article

Effect of Pore Thickness and the State of Polarization on the Optical Properties of Hexagonal Nanoarray of Au/Nanoporous Anodic Alumina Membrane

Mohamed Shaban

Nanophotonics and Applications (NPA) Laboratory, Department of Physics, Faculty of Science, Beni-Suef University, Salah Salem Street, Beni-Suef 62514, Egypt

Correspondence should be addressed to Mohamed Shaban; mssfadel@yahoo.com

Received 13 September 2015; Revised 22 November 2015; Accepted 30 November 2015

Academic Editor: Xuping Sun

Copyright © 2015 Mohamed Shaban. This is an open access article distributed under the Creative Commons Attribution License, which permits unrestricted use, distribution, and reproduction in any medium, provided the original work is properly cited.

Hexagonal nanoarrays of Au particles were deposited on nanoporous anodic alumina membrane (NAAM) utilizing r.f. magnetron sputtering. The thickness of the NAAMs is adjusted by changing the second anodization time from 5 min to 20 min. The surface morphology, composition, and optical properties are characterized by using SEM, EDX, and spectrophotometer, respectively. The effects of the NAAM thickness and state of polarization on the morphological changes and on the optical properties of the fabricated nanoarrays were addressed. According to the measured optical spectra, the rate of decrease of NAAMs refractive index was found to be 3.825×10^{-4} nm^{-1}. Using the modified Kubelka-Munk radiative transfer model, the energy gap of NAAMs was calculated from diffused reflectance and was decreased from 1.682 to 1.376 as the anodization time increased from 5 to 20 min. Also, the saturation of interference fringes is substantially enhanced, and field enhancement can be achieved due to the excitation and constructive interference of surface plasmon waves by coating NAAMs with the hexagonal nanoarrays of Au. Based on the advantages of the fabrication approach and the enhanced and controlled properties, this new generation of samples can be used as promising building blocks for nanophotonic and nanoelectronics devices.

1. Introduction

In recent years, porous materials have attracted much interest because of their potential use in a variety of applications [1–3]. Among them, nanoporous anodic alumina membranes (NAAMs) have been widely used as membranes in the fabrication of various nanostructures. Two-step anodization was widely used to fabricate NAAMs because of the high controllability of the process, cheap equipment, and facile technology [4]. Metal nanostructures are usually loaded to extend the application of porous membranes [5], so the conducting, mechanical, and optical properties of porous membranes could be improved [2]. Up to now, different kinds of nanotubes, nanorods, nanoparticles, and nanowires have been successfully synthesized inside the pores of NAAMs [6–8]. Homogenous deposition of metal nanostructures inside the pores of NAAMs has gained much attention in recent years. This attention is ascribed to their extensive use as substrates for sensors based on surface-enhanced Raman scattering (SERS), laser induced fluorescence (LIF), and electrochemical measurements [3, 9–11].

For an instant, the metal nanostructures on the outer surface of NAAMs have more possibility of touching the molecules that will be detected. Additionally, many reports have been done on optical properties of NAAMs [5, 12, 13]. NAAMs showed bright colors, but their saturation is very tiny. Colored nanostructures always have to be sealed with the nanopores of NAAMs to increase and modify the color saturation [12, 13]. Also, the optical properties of gold nanostructures have been extensively studied [5, 13–15]. Surface plasmon resonances interactions characterize these studies. These surface plasmon interactions can be used to enhance, guide, and modify the optical fields of novel nanoarrays such as photonic crystals [16], sensors based on SERS [10, 17], laser induced fluorescence, and near-field microscopy [3]. In particular, Au nanoarrays possess

features of both nanostructured metals that exhibit localized surface plasmon (LSP) excitations and planar metal films that exhibit propagating surface plasmon (PSP) excitations [5, 13, 18, 19]. Additionally the optical response of nanoparticle arrays depends on their size and shape. The interparticle coupling leads to energy shifts and splitting of degenerate modes, an effect that is prominent for regular nanoarrays.

In our previous studies, different metals have been loaded on the outer surface of NAAMs such as Au, Cr, Pt, and Sn [11, 13, 20, 21]. A controlled methodology of utilizing r.f. magnetron sputtering to coat NAAMs with hexagonal nanoarrays of Au nanoparticles was discussed [13]. Also, experimental studies of Au particles size, pore diameter, and angle of the incident were addressed. These studies showed the surface plasmon enhancement of NAAMs interference and illuminated the relationships between resonance position and structures (pore diameter and thickness) of porous gold layer and angle of incident.

However, there are other factors that can affect the optical properties of these nanostructures including the thickness of NAAM and the state of polarization of light. All of these factors make it important to have experimental data that can correlate the thickness of NAAMs and state of polarization with the optical properties. Here, we studied the optical properties of NAAMs of different thicknesses before and after decoration with hexagonal nanoarrays of Au particles under illumination with s- and p-polarized light.

2. Sample Fabrication and Characterization

Two-step anodization combined with a pore widening process was utilized to fabricate NAAMs with homogeneous pore diameters and high-quality pore walls [5, 22]. The 1st anodization process was performed at 40 V in 0.3 M oxalic acid at 10°C for 3 h. After the removal of the nanoporous Al_2O_3, the second anodization was performed at the same conditions for varying lengths of time followed by the barrier-thinning process. The barrier layer was thinned by a successive drop of the DC voltage from 40 to 15 V at a rate of 0.1 V/s and then maintained at 15 V for 5 min. The pore widening was carried out for 70 min pore widening after 10 min cathodic polarization [22]. Au nanoparticles were sputtered on the NAAMs using r.f. magnetron sputtering for 40 s [13]. The distance between the target and the substrate was 100 mm. Magnetron sputtering was carried out in pure Ar with a radiofrequency power of 65 W. The total pressure during deposition was 5.0 mTorr. The substrate temperature during the sputtering was set at room temperature.

Atomic force microscopy (AFM), field emission scanning electron microscope (FE-SEM, JSM-7500F/JEOL), and energy dispersive X-ray spectrometer (EDX, Oxford Link ISIS 300 EDX) were used to study the morphological and structural properties and chemical composition of the fabricated nanoarrays. Optical reflectance in the spectral range from 300 to 1000 nm was measured using UV/VIS/NIR 3700 double beam Shimadzu spectrophotometer at RT.

3. Results and Discussion

3.1. Morphological and Chemical Composition Studies. FE-SEM characterized the surface properties of the blank NAAMs. Figure 1(a) illustrates a typical FE-SEM top view of NAAM. Hexagonal aligned nanopores were formed in NAAM. The pore diameter is ~79 nm, the interpore distance is ~100 nm, and the pore density is $\sim 1.1 \times 10^{10}$ cm^{-2}. The inset of Figure 1(a) illustrates the defect map of this sample. The ratio of defects is 0.17. As shown in cross-sectional views of NAAM anodized for (b) 5 min and (c) 10 min, around each nanopore there is hexagonal arrangement from six active nanodots, which is consistent with the hexagonal packing structure of the pores. Because the farthest distances from the nanopores induced the weakest intensity of the electric field in the electrochemical process, then the oxidation rate is slowest resulting in the protuberances at special sites [23]. However, the number of defects or cracks decreased and homogeneity of the hexagonal arrangement increased as the second anodization increased. Then, the percentage of defects decreases and the averaged regularity ratio increases by increasing the anodization time, which is consistent with the literature data [24]. Additionally, from these images the rate of growth of the pores was found to be 1.3 nm/sec.

Figure 2 shows FE-SEM and AFM images of NAAMs of different thicknesses sputtered with Au under the same conditions for 40 sec. As shown from this figure, the homogeneity and hexagonal arrangement of the Au nanoparticles are improved by increasing the thickness of the starting NAAM. This may be attributed to the better arrangement of nanopores of the start NAAM and their active nanodots that was obtained with the longer second anodization time. As the Au particles grown around the active dots, the averaged pore diameters are decreased to 59 and 56 nm for Au nanoarrays that deposited on the 5 and 10 min anodized NAAMs, respectively. Also, the average Au particle diameters are increased from ~44 and 58 nm. Moreover, one can observe a slight increase in the averaged Au nanoparticles heights from ~39.5 to ~44.5 nm. This may be a result of the shorter distance between the surface of the substrate (NAAM) and the surface of Au target, due to the difference in the heights of the starting NAAMs. Then, for a longer anodization time, the Au nanoparticles are grown faster around the active dots, and the rate of lateral growth is faster than the rate of vertical growth. Moreover, the subgaps (holes) between the hexagonal Au nanoparticles grown on 5 min anodized NAAM are greater than that of the 10 min anodized NAAM.

To study the chemical composition of the fabricated sample, the Au/NAAMs were analyzed by EDX as shown in Figure 3. The EDX pattern exhibits the signals of Au, Al, and O elements. The quantitative results were 89.34% Al, 9.11% O, and 1.55% Au for the NAAMs anodized for 5 min. By increasing the anodization duration of the starting NAAMs from 5 to 10 min, the ratio of the Au is increased to 2.05%, consistent with the results of the analysis of AFM images in Figure 2.

3.2. Optical Properties of NAAM and Au/NAAM. Figure 4(a) shows reflectance spectra of NAAMs of different thicknesses.

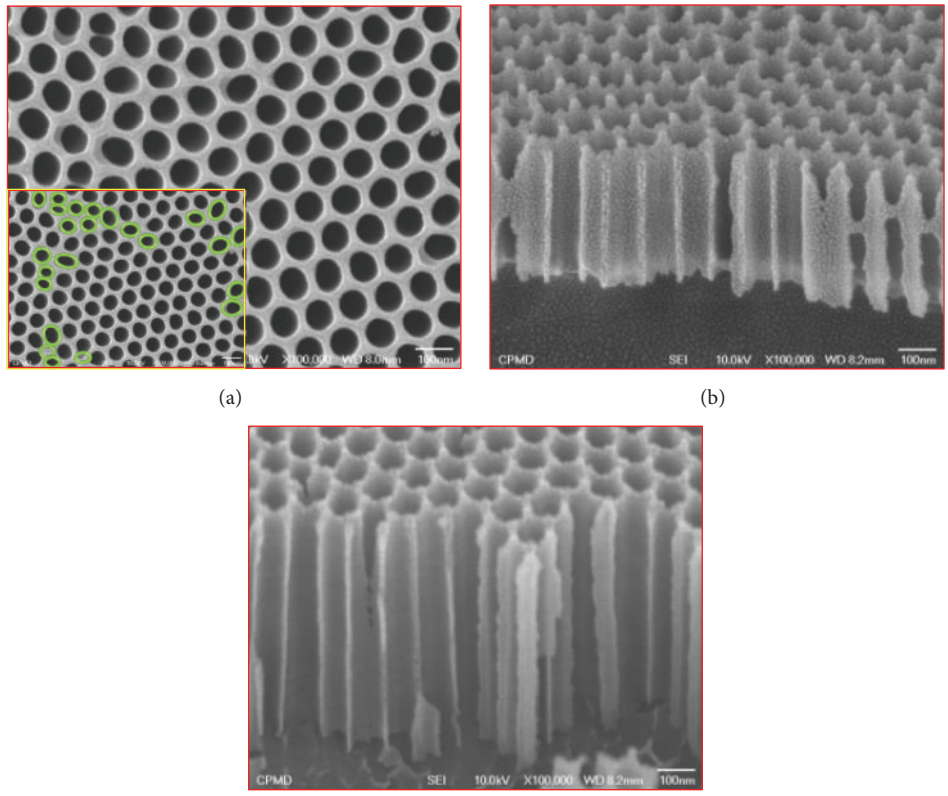

FIGURE 1: FE-SEM images (a) top view and cross-sectional view of NAAMs anodized for (b) 5 min and (c) 10 min. The inset of (a) shows the defect map of this sample. The scale bar is 100 nm.

The optical measurement geometry is shown in the inset schematic diagram of Figure 4(a). By increasing the membrane thickness, the number of interference ripples increases, which is consistent with Bragg's law. Increasing the thickness of NAAMs shifts the dips in the reflectance that occurs to longer wavelengths; these dips are originated from the destructive interference between the reflected waves from Al/NAAM and NAAM/air interfaces. As shown in the inset, the absorption band below 400 nm is associated with the decrease in the absorption coefficient. The average reflectivity of NAAMs, ~80%, is almost unchanged. This means that the scattering coefficient and hence the effect of scattering are minuscule and negligible for these NAAMs for wavelengths >400 nm. It is well known that the strength of interference ripple increases, as the wavelength increased; however, the interference ripple around 430 nm is much stronger. This may be a result of the blue emission band of NAAM which can be attributed to mixed emission from F and F^+ centers as discussed by Nasir et al. [25].

Figure 4(b) shows reflectance spectra measured for s- and the p-polarized light incident at an angle of 30° for NAAMs anodized in oxalic acid for 15 min. As shown in the figure a broad minimum centered at 470 nm for p-polarized light, which was originally located at 457 nm for s-polarized light. This indicates an increasing asymmetry for p-polarized light and the existence of two minima. To illustrate this point, the p-polarized spectrum has been normalized to the s-polarized spectra in the inset of Figure 4(b), revealing the existence of two minima at 415 and 488 nm.

Using Bragg's law and interference fringes in the reflectance spectra of Figure 4(a), the effective refractive indices, n_{eff}, can be calculated using [13]

$$n_{\text{eff}}^2 = \frac{\lambda_1^2 \lambda_2^2}{\left[4d^2 \left(\lambda_1 - \lambda_2\right)^2\right]} + \sin^2\theta, \tag{1}$$

where λ_1 and λ_2 are the wavelengths of two adjacent maxima or minima, $\theta = 30^\circ$ is the angle of incident, and d is the thickness of NAAM. The values of the order of interference, m_i, positions of reflectance dips or minima, λ_{res}, and effective refractive index are shown in Table 1. Figure 4(c) displays the linear decrease of an effective refractive index versus thickness of NAAM. From the linear fitting, the rate of decrease of refractive index is $3.825 \times 10^{-4}\,\text{nm}^{-1}$.

Using the diffused reflectance spectra, Figure 4(a), the band gap energy can be calculated by applying the modified Kubelka-Munk radiative transfer model [26]. From the measured reflectance spectra, the absorbance $A = R_{\text{max}} - R$, where R_{max} is the maximum value of reflectance for wavelengths longer than that of the dip in the diffuse reflectance and R is the reflectance. The calculated absorbance spectra are shown in Figure 4(d) for the NAAMs anodized for 5 and 15 min. The band gap wavelength and hence energy gap can be obtained by extrapolating the long-wavelength edge of the peak in

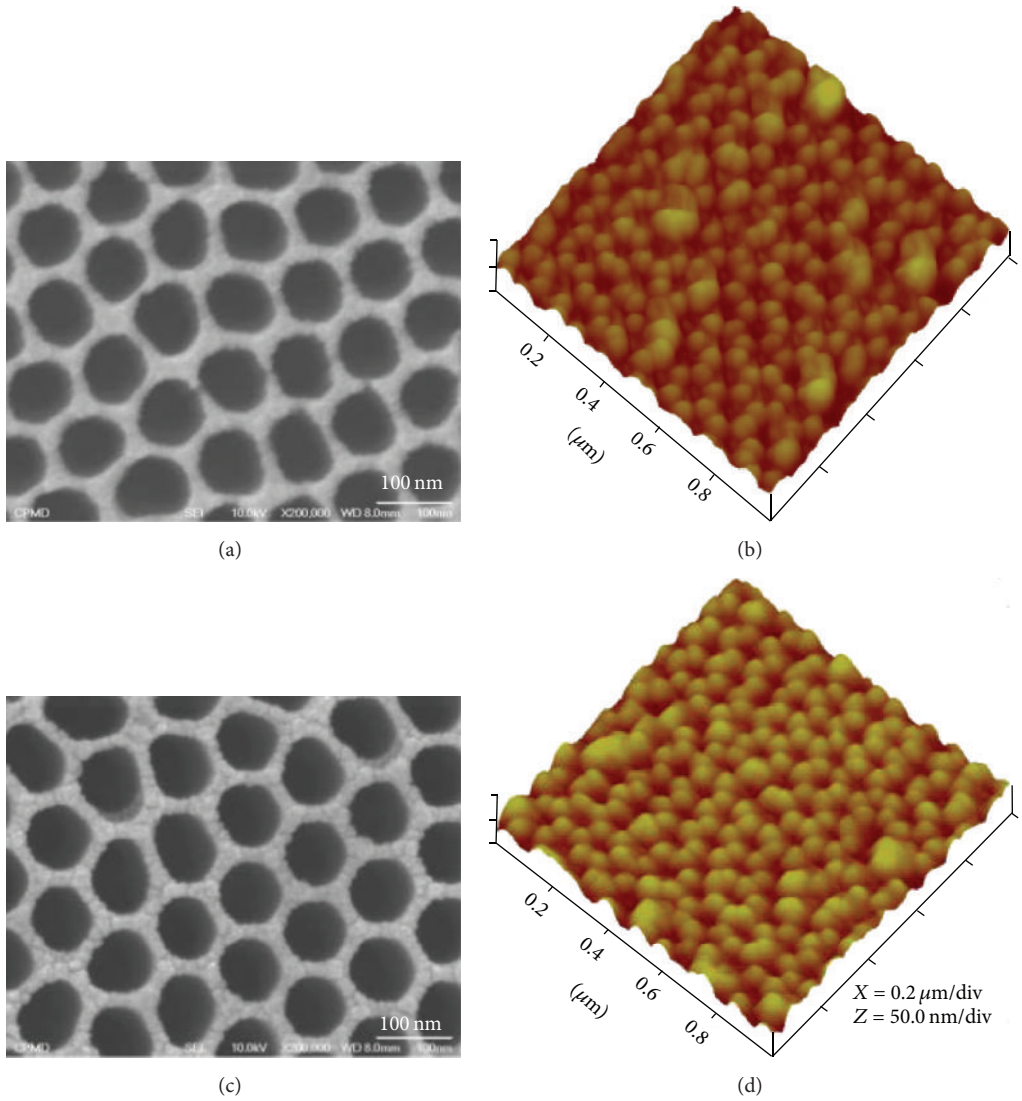

Figure 2: FE-SEM and AFM images of NAAMs anodized for ((a), (b)) 5 min and ((c), (d)) 10 min sputtered with Au for 40 sec under the same conditions.

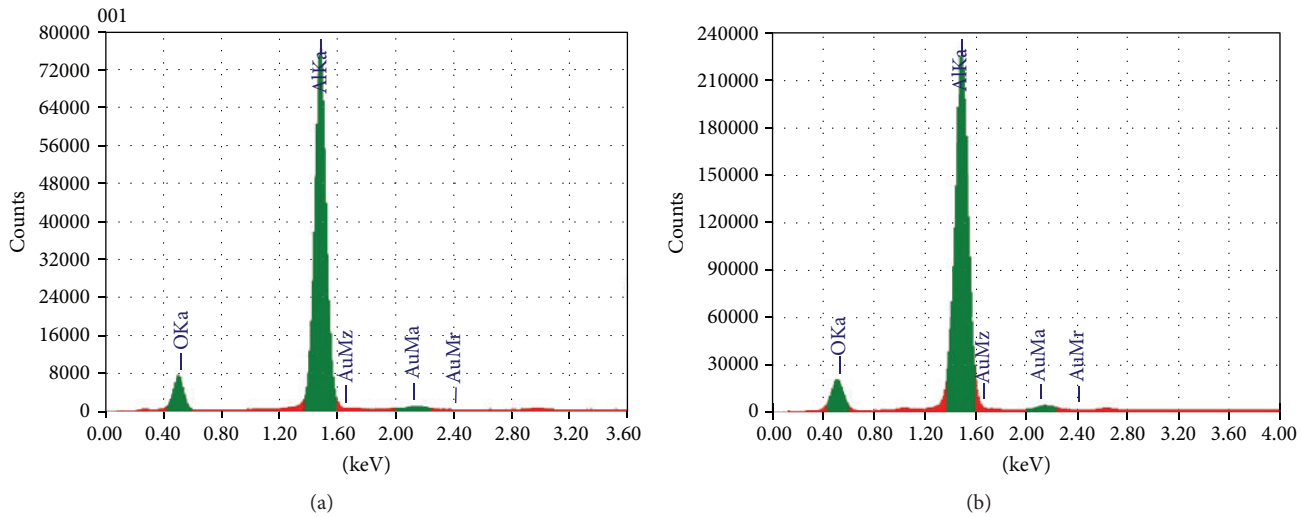

Figure 3: EDX spectra of the fabricated 40 s Au-coated NAAMs anodized for (a) 5 min and (b) 10 min.

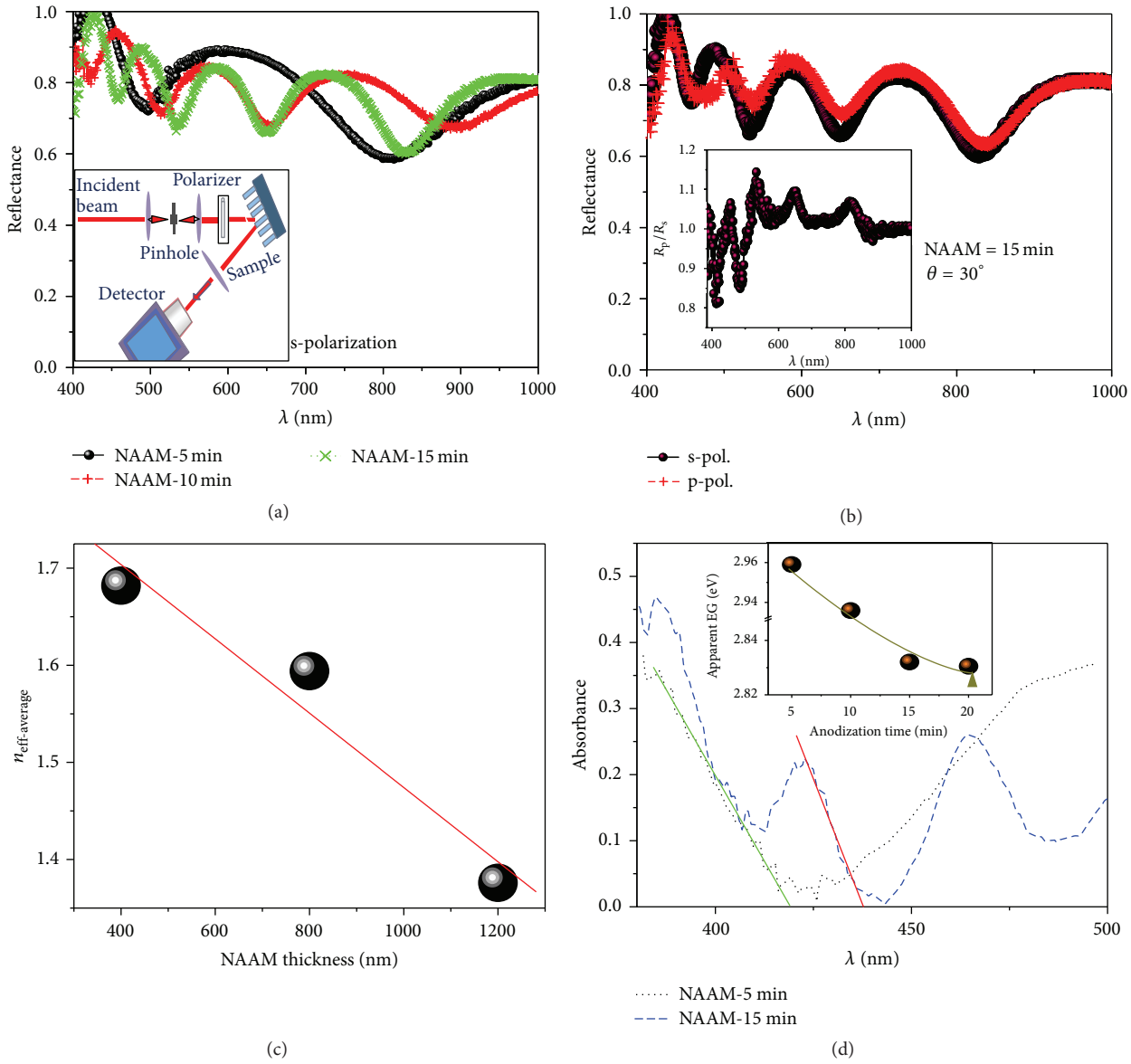

FIGURE 4: Optical properties of NAAMs (a) anodized for different times and (b) illuminated with various states of polarization, (c) variation of n_{eff} with the thickness of NAAM, and (d) calculated absorbance of NAAM showing linear extrapolations to obtain the band gap versus anodization time (the inset). The inset of (a) shows a schematic drawing of the optical setup.

TABLE 1: The values of the order of interference, m_i, positions of reflectance minima, λ_{res}, and the effective refractive index.

	AAO = 5 min		AAO = 10 min			AAO = 15 min				
	400 nm		800 nm			1200 nm				
m_i	2	1	4	3	2	1	4	3	**2**	**1**
λ_{res} (nm)	496	808	423	518	653	890	458	533	651	829
n_{eff}	1.682		1.526	1.644	1.612		1.445	1.323	1.359	
$n_{eff\text{-}aver}$	1.682		1.594				1.376			

absorbance to the zero line of absorbance. The variation of the obtained energy gap values with the anodization time is shown in the inset of Figure 4(d). The energy gap is decreased from 1.682 to 1.376 as the anodization time increased from 5 to 20 min.

To emphasize the role of Au nanoparticles in the modulation of the reflective spectroscopic response of the studied NAAMs, the samples were sputter-coated with Au.

The reflectance spectra of 40 s Au-coated NAAMs anodized in oxalic acid for 5, 10, and 15 min are shown in

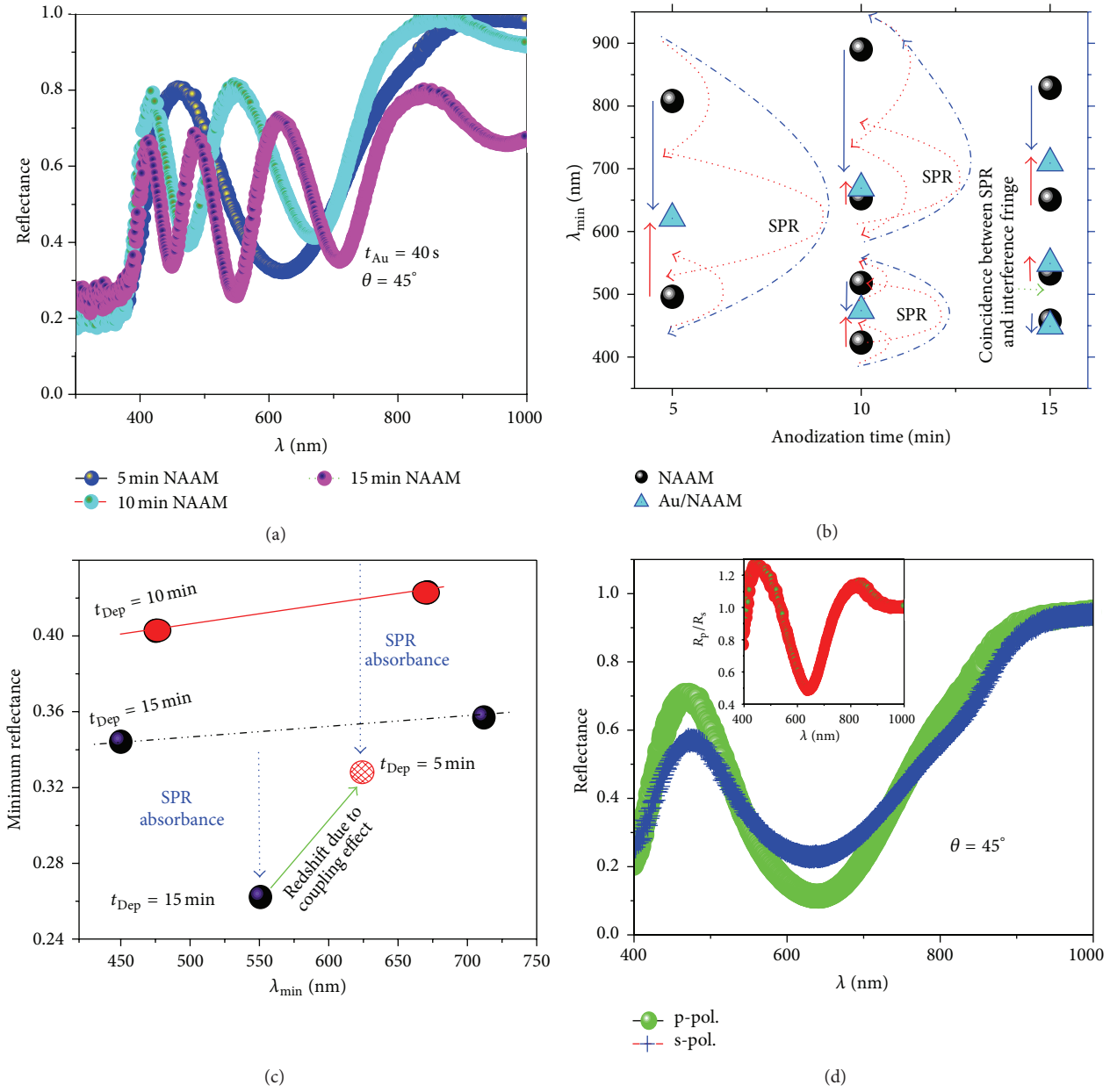

FIGURE 5: (a) Reflectance spectra of 40 s Au-coated NAAMs anodized for different lengths of time, (b) λ_{min} versus the anodization time for NAAM (black spheres) and Au/NAAM (blue triangles), (c) minimum reflectance versus λ_{min}, and (d) reflectance spectra of Au/NAAM illuminated with s- and p-polarized light incident at an angle of 45°. The inset shows the dependence of R_p/R_s on the wavelength.

Figure 5(a). As shown in the figure, all three samples exhibit strong oscillations; these oscillations result from surface plasmon enhancement of optical interference between the light beams that reflected from the top and bottom surfaces of the sample. With increasing thickness of NAAMs, the number and the position of interference bands increase, while their bandwidth and reflectivity decrease. The distance between interference bands increases as the wavelength is increased. Additionally, the oscillation amplitude decreases with decreasing wavelength, and the rate of decrease is sample dependent. The data shows that a reduced anodizing time (NAAM thickness) will lead to more pronounced interference; this may be ascribed to a more efficient SPR propagation at the metal/dielectric interface in addition to the decrease of the dielectric layer thickness. The strong enhancement of the plasmon field occurs at contacting surfaces between Au nanoparticles and leads to super-focusing of electromagnetic waves. Then, the reflected waves of NAAMs are strongly modulated by hexagonal arrays of Au nanoparticles and the oscillation strength (the difference between the maximum and minimum) of interference fringes is increased.

Figure 5(b) shows the position of the characteristic minima (λ_{min}) versus the anodization time for NAAM (black spheres) and Au/NAAM (blue triangles). This figure summarizes the red- and blueshifts that happened for all

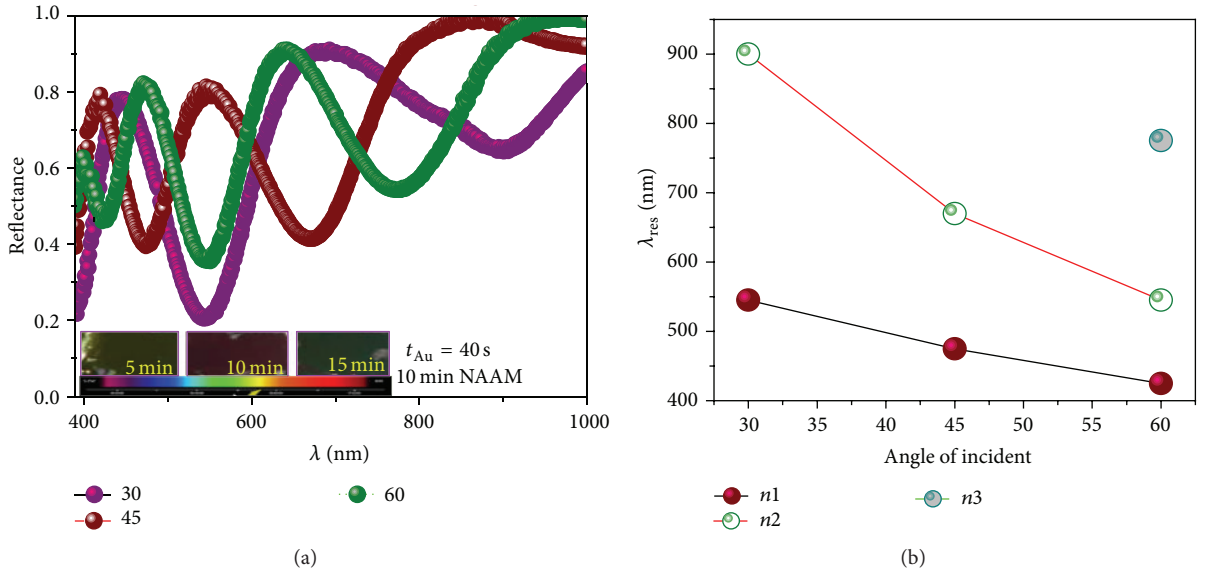

FIGURE 6: Reflectance spectra of 40 s Au/NAAM measured at different angles. The inset shows photographs captured at the normal incident.

the characteristic minima as a result of the coupling between interference fringes and Au surface plasmon resonances (SPRs). When the coincidence between the position of interference fringe and SPR occurs, the absorbance will be enhanced at that position and strong absorption band is noted in the reflectance spectra [5, 13]. Figure 5(c) shows the minimum reflectance versus λ_{min} for the characteristic minima. This figure clearly illustrates that the strongest absorption band is located around 550 nm for 40 s Au/15 min NAAM sample. Then, this minimum is affected by LSPR more than other minima. This indicates that the position of the SPR for this sample is located very close to 550 nm. By decreasing the anodization time to 5 min, LSPR is redshifted. This redshift is ascribed to the negative dipole-dipole coupling energy contribution due to the lack of the direct conductive interlink between Au nanoparticles [13].

Figure 5(d) shows reflectance spectra measured for s- and the p-polarized light incident at an angle of 45° for 40 s Au-coated NAAM anodized in oxalic acid for 5 min. As shown in the figure a broad minimum centered at 642 nm for p-polarized light and 635 nm for s-polarized light; however, the effect was more pronounced for p-polarized light, which shows an increasing asymmetry. The broad minimum appears to be due to the existence of two minima: the first is similar to that seen in the s-polarized light and the second is sharper than the first one and occurs very close to it. To illustrate this point, the p-polarized spectrum has been normalized to the s-polarized spectra in the inset of Figure 5(d), revealing a minimum at a wavelength of 638 nm. For nanoparticles that are in direct contact or a few nanometers apart, direct electronic coupling occurs as a result of the overlap of electronic wave functions [27]. These electronic exchange reactions are resulting in redshift and broadening of the plasmon resonance compared to that of noninteracting particles. For s-polarized light, the electric field vector had only one component parallel to the surface of the Au array and excited the electron oscillation in the same plane. For p-polarized light, an additional normal component appears at an oblique angle and excited electron oscillations normal to the plane of the Au array on the top surface of NAAM in addition to the parallel electron oscillations. Therefore, the redshift and broadening were attributed to the plasmon coupling of these normal oscillations.

Recently, structural colors have attracted much interest because their applications have been rapidly progressing in many fields related to vision and decoration purposes [28]. Most of the structure colors originate from fundamental optical processes including thin-film interference, multilayer interference, diffraction grating effect, photonic crystals, and light scattering [28]. We noticed that the coated Au-NAAMs used in this study have a brilliant color with high saturation caused by the surface plasmon enhancement of optical interference, as we discussed in a previous report [13]. This is evident from Figure 6, where the effect of angle of incident and normal incident-photographs of decorated membranes are shown. As shown in the figure, the samples possess obvious structural color and have strong light mirroring in a certain wavelength. It has been found that the sample color is mainly affected by the thickness of NAAM (anodizing time). Note that the color of the samples changes with different viewing angles because they are derived from interference. Also, as the angle of incident increases, the number of fringes is increased but the oscillation strength and the fringe width are decreased. The variation of the resonance minima wavelength with the angle of incident is shown in Figure 6(b). As the angle of incident increased, λ_{res} is blueshifted.

4. Conclusion

In conclusion, we have successfully coated NAAMs of different thicknesses with nanoporous hexagonal Au particles. The morphologies, structures, and chemical composition of

NAAMs and Au/NAAMs are studied by FE-SEM, AFM, and EDX. The defects percentage decreases and the averaged regularity ratio increases by increasing the anodization time. The average Au particles diameters are increased from ~44 to 58 nm, and the Au nanoparticles heights are also increased from ~39.5 to ~44.5 nm as the anodization time increased from 5 to 10 min. From the reflectance of the blank NAAM, s-polarized light shows a sharp minimum at 457 nm. However, p-polarized light showed a broad minimum centered at 470 nm that originally results from the existence of two minima at 415 and 488 nm. This indicates an increasing asymmetry for p-polarized light. The effective refractive index of NAAMs is linearly decreased with the thickness of NAAM, and the rate of decrease was found to be 3.825×10^{-4} nm^{-1}. Using the modified Kubelka-Munk radiative transfer model, the energy gap of NAAMs is decreased from 1.682 to 1.376 as the anodization time increased from 5 to 20 min. For 40 s Au-coated NAAMs, the number and the position of the strong interference bands increase while their bandwidth and reflectivity decrease as the NAAM thickness increased. Additionally, the oscillation strength and oscillation width decrease with decreasing wavelength. The samples possess obvious structural color and have strong light mirroring in a certain wavelength. The advantages of the fabrication approach and the enhanced and controlled optical properties make these samples suitable for nanophotonic and nanoelectronics devices.

Conflict of Interests

The author declares that there is no conflict of interests regarding the publication of this paper.

Acknowledgment

This work was partially supported by the Science and Technology Development Fund (STDF) Program of Egypt (Grant no. 4617).

References

[1] C. W. Lai, "Surface morphology and growth of anodic titania nanotubes films: photoelectrochemical water splitting studies," *Journal of Nanomaterials*, vol. 2015, Article ID 820764, 7 pages, 2015.

[2] D. Losic and A. Santos, *Electrochemically Engineered Nanoporous Materials: Methods, Properties and Applications*, vol. 220 of *Springer Series in Materials Science*, Springer, Basel, Switzerland, 2015.

[3] M. Shaban, A. M. Ahmed, E. Abdel-Rahman, and H. Hamdy, "Fabrication and characterization of micro/nanoporous Cr film for sensing applications," *Microporous and Mesoporous Materials*, vol. 198, pp. 115–121, 2014.

[4] X. Y. Han and W. Z. Shen, "Improved two-step anodization technique for ordered porous anodic aluminum membranes," *Journal of Electroanalytical Chemistry*, vol. 655, no. 1, pp. 56–64, 2011.

[5] M. Shaban, H. Hamdy, F. Shahin, and S.-W. Ryu, "Strong surface plasmon resonance of ordered gold nanorod array fabricated in porous anodic alumina template," *Journal of Nanoscience and Nanotechnology*, vol. 10, no. 5, pp. 3034–3037, 2010.

[6] M. R. Kim, D. K. Lee, and D.-J. Jang, "Template-based electrochemically controlled growth of segmented multimetal nanorods," *Journal of Nanomaterials*, vol. 2010, Article ID 203756, 7 pages, 2010.

[7] C. Y. Han, Z.-L. Xiao, H. H. Wang, X.-M. Lin, S. Trasobares, and R. E. Cook, "Facile synthesis of highly aligned multiwalled carbon nanotubes from polymer precursors," *Journal of Nanomaterials*, vol. 2009, Article ID 562376, 11 pages, 2009.

[8] M. Shaban, M. Ali, K. Abdel-Hady, and H. Hamdy, "Al_2O_3 and Sn/Al_2O_3 nanowires: fabrication and characterisation," *Micro & Nano Letters*, vol. 10, no. 7, pp. 324–329, 2015.

[9] G. Wang, C. Shi, N. Zhao, and X. Du, "Synthesis and characterization of Ag nanoparticles assembled in ordered array pores of porous anodic alumina by chemical deposition," *Materials Letters*, vol. 61, no. 18, pp. 3795–3797, 2007.

[10] D. Sung, S. Hong, Y.-H. Kim et al., "Ab initio study of the effect of water adsorption on the carbon nanotube field-effect transistor," *Applied Physics Letters*, vol. 89, Article ID 243110, 2006.

[11] M. Serry, A. Gamal, M. Shaban, and A. Sharaf, "High sensitivity optochemical and electrochemical metal ion sensor," *Micro and Nano Letters*, vol. 8, no. 11, pp. 775–778, 2013.

[12] Y. Yamamoto, N. Baba, and S. Tajima, "Coloured materials and photoluminescence centres in anodic film on aluminium," *Nature*, vol. 289, pp. 572–574, 1981.

[13] M. Shaban, H. Hamdy, F. Shahin, and S.-W. Ryu, "Optical properties of porous anodic alumina membrane uniformly decorated with ultra-thin porous gold nanoparticles arrays," *Journal of Nanoscience and Nanotechnology*, vol. 11, no. 2, pp. 941–952, 2011.

[14] H. Li, C. Kan, Z. Yi, X. Ding, Y. Cao, and J. Zhu, "Synthesis of one dimensional gold nanostructures," *Journal of Nanomaterials*, vol. 2010, Article ID 962718, 8 pages, 2010.

[15] R. Nikov, N. Nedyalkov, P. A. Atanasov, M. Terakawa, H. Shimizu, and M. Obara, "Tuning the optical properties of gold nanostructures fabricated on flexible substrates," *Applied Surface Science*, vol. 264, pp. 779–782, 2013.

[16] X. Zhang, B. Sun, H. Guo, N. Tetreault, H. Glessen, and R. H. Friend, "Large-area two-dimensional photonic crystals of metallic nanocylinders based on colloidal gold nanoparticles," *Applied Physics Letters*, vol. 90, no. 13, Article ID 133114, 2007.

[17] M. Shaban, A. G. A. Hady, and M. Serry, "A new sensor for heavy metals detection in aqueous media," *IEEE Sensors Journal*, vol. 14, no. 2, pp. 436–441, 2014.

[18] X. Lang, L. Qian, P. Guan, J. Zi, and M. Chen, "Localized surface plasmon resonance of nanoporous gold," *Applied Physics Letters*, vol. 98, no. 9, Article ID 093701, 2011.

[19] L. H. Qian, X. Q. Yan, T. Fujita, A. Inoue, and M. W. Chen, "Surface enhanced Raman scattering of nanoporous gold: smaller pore sizes stronger enhancements," *Applied Physics Letters*, vol. 90, no. 15, Article ID 153120, 2007.

[20] M. Shaban, H. Hamdy, F. Shahin, and S.-W. Ryu, "Fabrication of ordered Cr nanostructures by self agglomeration on porous anodic alumina membranes," *Journal of Nanoscience and Nanotechnology*, vol. 11, no. 8, pp. 7145–7150, 2011.

[21] M. Shaban, M. Ali, K. Abdel-hady, and H. Hamdy, "Self-agglomeration of tin nanoparticle array on porous anodic alumina membranes: fabrication and characterization," *Current Nanoscience*, vol. 11, no. 2, pp. 214–221, 2015.

[22] M. Shaban, H. Hamdy, F. Shahin, J. Park, and S.-W. Ryu, "Uniform and reproducible barrier layer removal of porous anodic alumina membrane," *Journal of Nanoscience and Nanotechnology*, vol. 10, no. 5, pp. 3380–3384, 2010.

[23] N. Ji, W. Ruan, Z. Li, C. Wang, Z. Yang, and B. Zhao, "A potential commercial surface-enhanced Raman scattering—active substrate: stability and usability," *Journal of Raman Spectroscopy*, vol. 44, no. 1, pp. 1–5, 2013.

[24] W. J. Stepniowskia, A. N. Stępniowskab, A. Preszc, A. Preszc, T. Czujkoa, and R. A. Varin, "The effects of time and temperature on the arrangement of anodic aluminum oxide nanopores," *Materials Characterization*, vol. 91, pp. 1–9, 2014.

[25] M. E. Nasir, B. Hamilton, and D. W. E. Allsop, "Optical measurements of nanoporous anodic alumina formed on Si using novel X-ray spectroscopy set up CLASSIX," *Nuclear Instruments and Methods in Physics Research—Section B: Beam Interactions with Materials and Atoms*, vol. 268, no. 3-4, pp. 251–253, 2010.

[26] A. B. Murphy, "Band-gap determination from diffuse reflectance measurements of semiconductor films, and application to photoelectrochemical water-splitting," *Solar Energy Materials & Solar Cells*, vol. 91, no. 14, pp. 1326–1337, 2007.

[27] C. Sun and X. Zhang, "The influences of the material properties on ceramic micro-stereolithography," *Sensors and Actuators A: Physical*, vol. 101, no. 3, pp. 364–370, 2002.

[28] S. Kinoshita and S. Yoshioka, "Structural colors in nature: the role of regularity and irregularity in the structure," *ChemPhysChem*, vol. 6, no. 8, pp. 1443–1459, 2005.

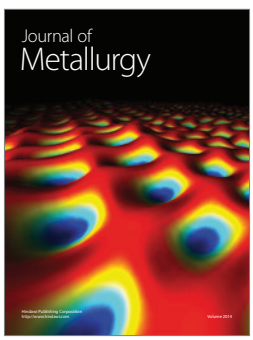

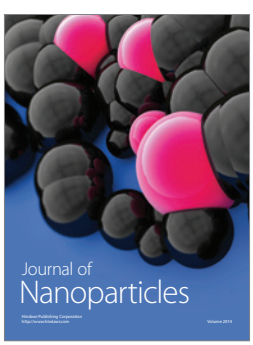

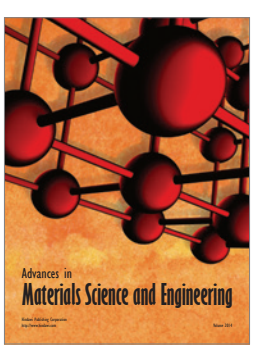

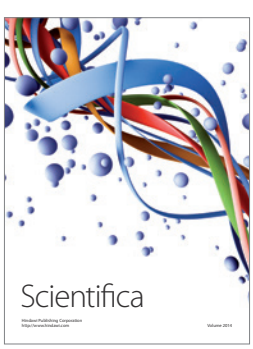

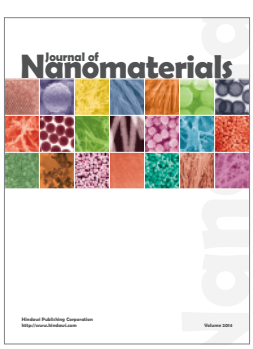

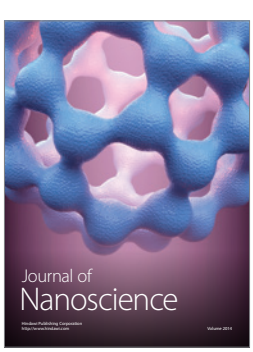

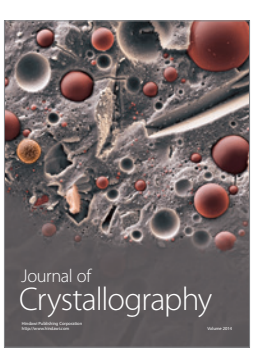

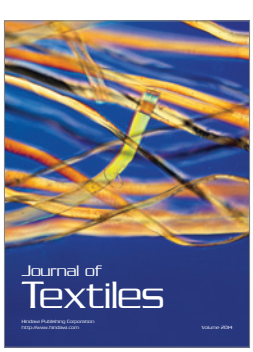

Hindawi

Submit your manuscripts at
http://www.hindawi.com